Transactions of the Institute of Measurement and Control 29, 3/4 (2007) pp. 215–253

Body segment position reconstruction and posture classification by smart textiles

A. Tognetti, R. Bartalesi, F. Lorussi and D. De Rossi

Interdepartmental Research Centre 'E. Piaggio', University of Pisa, Via Diotisalvi 2, 56126, Pisa, Italy

Textile-based transducers are an innovative category of devices that use conductive fibres meshed with elastic textile fabrics. Within this paper, a new class of strain sensors, which represents an excellent trade-off between figures of merit in mechano-electrical transduction and possibility of integration in textiles, is presented. Electrically conductive elastomer composites show piezo-resistive properties when a deformation is applied. Conductive elastomer can be applied to fabric or to other flexible substrate and they can be employed as strain sensors. We integrated conductive elastomer sensors into fabrics to realize wearable kinaesthetic garments able to detect posture and movement of a user. This paper deals with the design, the development and realization of a set of sensing garments, from the characterization of innovative textile-based sensors to the methodologies employed to gather information on the posture and movement from the entire garments. Data deriving from the prototypes are analysed and compared with those deriving from a traditional movement tracking system. The realized kinaesthetic garments have shown very promising performance in terms of body segment position reconstruction and posture classification.

Key words: posture classification; textile sensors; wearable technology.

1. Introduction

The development of new technologies in smart fibre and fabric manufacturing allows the embedding of functionalities into common-use objects such as garments (Dunne *et al*., 2005a; Scilingo *et al*., 2005; Steele and Wallace, 2002; Tognetti *et al*., 2005) or shoes (Morris and Paradiso, 2002; Pappas *et al*., 2004; Press release, 2004). These functions

Address for correspondence: Alessandro Tognetti, Interdepartmental Research Centre 'E. Piaggio', University of Pisa, Via Diotisalvi 2, 56126, Pisa, Italy. E-mail: a.tognetti@ing.unipi.it
Figures 1–7, 9, 13, 14 and 16–24 appear in colour online: http://tim.sagepub.com

 10.1177/0142331207069487

can cover all kinds of tasks, such as monitoring the status of a human subject or generating forces to ensure a bi-directional communication among humans and machines. In particular, physiological and biomechanical variable acquisition has become available by several textile-based prototypes (Dunne *et al*., 2005a; Gibbs and Asada, 2005; Scilingo *et al*., 2005; Steele and Wallace, 2002; Tognetti *et al*., 2005).

Studies on customers' acceptance and on receptivity to health benefits delivered through clothing point out approvals toward qualities such as comfort, good fit, ease of care, breathability and a good texture (additionally, they also would like a youthful stylish fashion). With those directives, techniques involved in the development of so-called *intelligent biomedical clothing* must realize devices that are affordable, user-friendly, inconspicuous, autonomous in terms of power consumption and able to assist individuals in their own health management (Dunne *et al*., 2005b; Lymberis and De Rossi, 2004). Textile technologies are widely considered one of the key factors toward pervasive computing (Marculescu *et al*., 2003).

What this paper describes is a new class of strain sensors, which represents an excellent trade-off between figures of merit in mechano-electrical transduction and possibility of integration in textiles. This work deals with an application of this technology to reconstruction of body posture and gestures.

In these fields, a large number of different techniques have been developed and tested. From a technical point of view, it is possible to classify devices by taking account of sensor position, power source and communication equipment with respect to the body segments whose properties have to be studied (Motion tracking tutorial). A classical, widely used and well-described class of systems devoted to motion detection is constituted by the set of optical-based motion analysis systems (Vicon motion systems; Zakotnik *et al*., 2004), magnetic tracking systems (Polhemus fastrak) or electro-goniometers (Biometrics electro-goniometers). These systems are accurate but they operate in a restricted area or they require the application of obtrusive parts on the subject's body. For these reasons, they are not suitable for a long-term on-body monitoring.

On the other hand, the development of new wearable analysis systems enables engineers to design systems that satisfy the user's requirements of wearability and long-term monitoring. Current prototypes realized by these emergent technologies use exoskeletal transducers or textile-based transducers.

In the first category, we can group accelerometer- and magnetometer-based devices. They are widely used in measuring multi-axis joint angles between body segments (Bouten *et al*., 1997; Fontaine *et al*., 2003) or in determining the activity of human subjects (Lukowicz *et al*., 2002; Van Laerhoven *et al*., 2002, 2003). Information provided by these sensors is accurate and continuous, but biomechanical reconstruction in terms of joint angles is actually difficult, strongly dependent on sensor location and limited to static applications (Fontaine *et al*., 2003). Moreover, using off-the-shelf sensors to realize these devices can make them uncomfortable and invasive.

Textile-based transducers are an innovative category of devices that use conductive fibres meshed with elastic textile fabrics. They usually satisfy wearability requirements and are used in real-time information gathering systems. This second category includes knitted fibre transducers (KFTs), sewn fibre transducers (SFTs) and smeared conductive elastomer (CE) transducers.

Resistive KFTs (Wijesiriwardana *et al*., 2003) permit the realization of garments with good mechanical properties. Transduction is realized by exploiting fibre piezo-resistivity. The difficulty in modelling the complex and non-isotropic relation between stretching and resistance in the weft-knitted loop does not yet permit applications in motion analysis. Anyway, they find applications in cardiopulmonary sign monitoring (Loriga *et al*., 2005). Encouraging results in terms of biomechanical reconstruction have been produced by using inductive KFT transducers (Wijesiriwardana *et al*., 2004). The use of SFTs in posture and movement analysis is described in Gibbs and Asada (2005). Garments realized with this technique satisfy wearability requirements but their application currently consist of single DOF monitoring because of the sensor dimensions. Finally, CE transducers are presented in this work and provide many interesting aspects that will be described in the next sections.

2. Materials and fabrication technologies

Electrically conductive elastomer (CE) composites show piezo-resistive properties when a deformation is applied. CEs can be applied to fabric or to other flexible substrate and they can be employed as strain sensors. We integrated CE sensors into fabrics to realize wearable kinaesthetic garments able to detect the posture and movement of a user.

2.1 Conductive elastomer sensors

The CE we used is a commercial product by Wacker Ltd (Elastosil LR 3162 A/B) and it consists of a mixture of graphite and silicon rubber. Wacker Ltd guarantees the non-toxicity of the product that, after vulcanization, can be employed in medical and pharmaceutical applications. It can be smeared on flexible and elastic substrate (as a fabric; De Rossi *et al*., 2002) or arranged in a film applicable on elastic supports.

Sensors have been realized by directly smearing the Wacker's CE on fabric (Lycra/cotton) previously covered by an adhesive mask, according to the shape and the dimension desired for the sensors. Then, the treated fabric is placed in an oven at about 130°C. During this phase, the cross-linking of the solution speeds up and in about 10 min, the sensing fabric is ready to be employed. CE sensors (Figure 1) do not change the mechanical properties of the elastic fabric on which they are applied and they can be used as strain sensors for high deformation measurement.

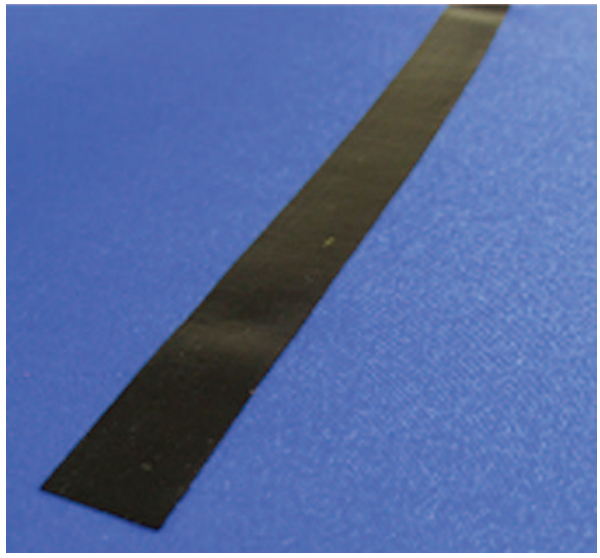

Figure 1 Smeared CE sensor

2.2 Kinaesthetic garments

CE sensors can be employed to realize wearable sensing systems able to record and detect human postures and gestures. Our main aim has been to produce a kinaesthetic garment collection, which can be worn for a long time with no discomfort. As a fundamental requirement for this, we have estimated the employment of a material that does not substantially change the mechanical properties of the fabric and maintains the wearability of the garment. To obtain this result, we have integrated sensor networks made by CE into elastic fabrics used to manufacture the kinaesthetic garment collection. In particular, two different kinaesthetic garments have been realized and will be described as follows:

- a sensorized shirt for the analysis of the upper limb kinematic configuration, namely the 'upper limb kinaesthetic garment' (ULKG);
- a sensorized glove for hand posture and gesture detection.

Printing both the set of sensors and connecting wires directly onto the fabric by using the same material (Figure 2, as an example) is a definite merit of our approach. In early prototypes (De Rossi *et al*., 2002; Figure 3), interconnections were constituted by metallic wires (Scilingo *et al*., 2003), which could bound movements and create motion artefacts. In this section, the whole design and realization process of kinaesthetic garments is described. In particular, we describe:

- the sensorized fabric realization (Section 2.2.1);
- the determination of the position and the orientation of sensors around the joints being monitored (Section 2.2.2);

Figure 2 Particulars of the sensorized glove. Sensors and connections to the electronic acquisition unit are made by using CE. Metallic wires are needed only in the periphery of the glove. In this way, movements of the hand are unbounded

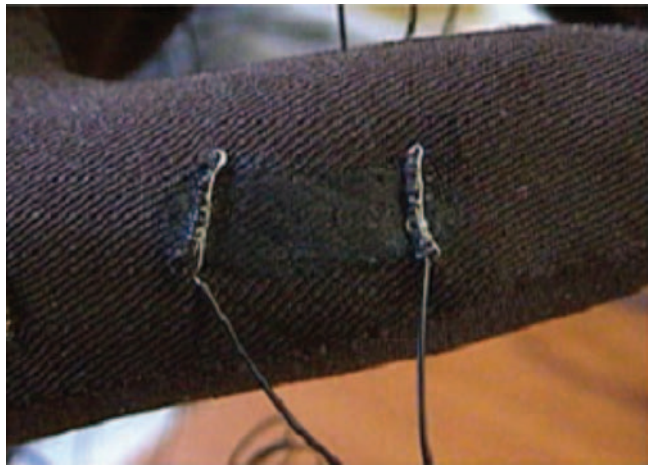

Figure 3 The sensorized glove. Sensors (in this figure is reported a sensor on the thumb) were connected to the acquisition unit with metallic wires

- the design of the mask used to obtain the desired sensor network topology on the fabric (Section 2.2.3); and
- the acquisition hardware design (Section 2.4).

2.2.1 Sensorized fabric realization: In the production process of a sensorized fabric, a solution of Elastosil diluted in trichloroethylene is smeared on the textile substrate as described in Section 2.1. The mask is designed according to the desired sensor network topology.

In Figure 4, the production process to obtain a fabric for a sensorized glove is represented: Figure 4a shows the adhesive mask drawing, used selectively to smear the solution composed of Elastosil–trichloroethylene on the substrate. The picture exactly corresponds to the desired geometry of the CE sensor network. This mask is obtained by cutting a sheet of adhesive paper according to the drawing of Figure 4a, which is then stuck on the fabric (Figure 4b) to smear the solution in selected parts (Figure 4c). After the material cross-linking, the mask is removed (Figure 4d) and the desired topology is impressed on the fabric.

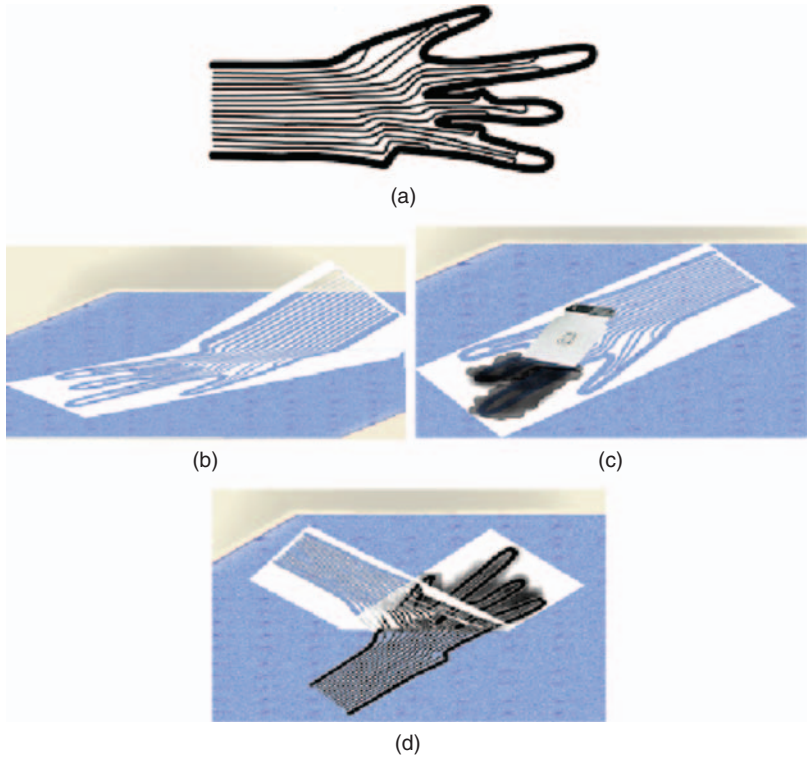

Figure 4 Application of a CE sensor network on a Lycra substrate to realize a kinaesthetic garment (glove). This process is the same for each kinaesthetic garment realized

2.2.2 Sensor topology: position and orientation: Sensor topology is a fundamental topic in the design of a sensing system that has to resolve a large number of degrees of freedom (DOFs). A fundamental remark on the matter states that a redundant number of sensors (ie, a number of sensors larger than the dimension of the space to monitor) uniformly spread around the joints can provide enough information to infer the essential features concerning the posture of a subject. This methodology neglects the exact sensor location in favour of their number. We borrow this approach from biological paradigms (De Rossi *et al*., 2003; Lorussi *et al*., 2004). Notwithstanding, because of the limited number of acquisition channels we have, the determination of sensor positions and orientations is an important issue. An heuristic approach has been adopted: by realizing a sensorized fabric sample and by placing it around the considered joints during the execution of natural movements, we have determined the set of positions and orientations that produced meaningful outputs in terms of movement reconstruction.

2.2.3 Design of the mask: The determination of the correct position and orientation of sensors according to the criteria exposed in Section 2.2.2 led us to design the adhesive mask used to smear sensors and the galley proofs used to connect the sensing network to the electronic acquisition system. The realization of the mask for the sensing glove (Figure 4a) is a simple issue. To obtain it, it is necessary to have a graphical model of the hand, which represents in two dimensions its anthropometrical variables (length of the bones, width of the palm, etc.). In this way, we can design the mask according to the appropriate sensor position. Conversely, the realization of the mask necessary for the ULKG (Figure 5) is a more complex task. In this case, the two-dimensional drawing of the mask has to match with the three-dimensional complexity of human anatomy. To guide us in finding a correspondence between the CE network location on the mask and on the garment, a three-dimensional model of the human body, used to trace the estimated sensor positions and then report them on a bi-dimensional map has been used.

2.3 Prototypes

2.3.1 Upper limb kinaesthetic garment: The ULKG prototype shown in Figure 6 has been realized by using the mask shown in Figure 5, and by printing the CE sensors and the connecting tracks on a Lycra/cotton fabric. In order to employ the same CE material both for sensors and for tracks, a dedicated topology was used. In this way, no conventional and cumbersome cables are necessary to connect the sensors to the electronics. As widely explained in Section 2.4, the bold black track in Figure 5 represents the set of sensors connected in series (S_i) and it covers the most important joints of the upper limb. The thin tracks (R_i) represent the connection between sensors and the electronic acquisition system. Since thin tracks are realized by the same CE material, they undergo a significant change in electrical resistance when limbs move.

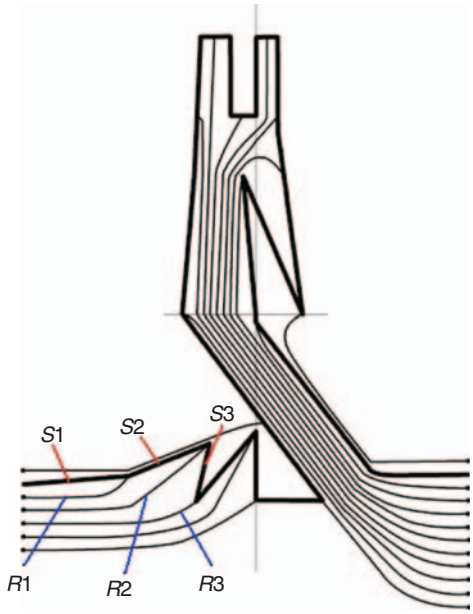

Figure 5 The mask used for the UKLG realization

Figure 6 Upper limb kinaesthetic garment (ULKG) prototype

For this reason the front-end electronic unit is designed to compensate for this variation, as Section 2.4 reports. Practically, a sensor S_i consists of a segment of the bold track between two consecutive thin track intersections. All these remarks on the ULKG also hold for the other prototypes.

2.3.2 Sensorized glove: Sensors and wires have been printed on a Lycra/cotton glove (Figure 2) by using the mask in (Figure 4a). The bold black track of Figure 4(a) and of Figure 2 represents the set of sensors connected in series and covers the most important joints of the hand. In the same way, a sensor consists of a segment of the bold track between two consecutive thin tracks (Figure 4a). This configuration is the evolution of an earlier prototype, where the connections between sensors and the acquisition device were realized by means of metallic wires, which could bound movements (Figure 3).

2.4 Kinaesthetic garments' electrical model and implementation of the acquisition technique

The electrical model of the ULKG is reported in Figure 7. For reasons explained in Section 2.3.1, the analogue front end of the electronic unit is designed to compensate for the resistance variation of the thin tracks during fabric deformations. A generator supplies the series of sensors S_i with a constant current I and the acquisition system is provided by an high input impedance stage realized by instrumentation amplifiers, represented in Figure 7 by the voltmeters. Thanks to this configuration, only small current flows through the connecting wires and the voltages which fall on R_i are negligible if the current I is big enough:

$$V_{n_i} \approx V_{m_i} \tag{1}$$

In conclusion, the voltages measured by the instrumentation amplifiers are equal to the voltages that fall on the S_i that are related to the resistances of the sensors. In this way, the thin CE tracks act as leads and a sensor, consisting of a segment of the bold track between two thin tracks, and can be smeared in any position to detect the movements of a certain joint.

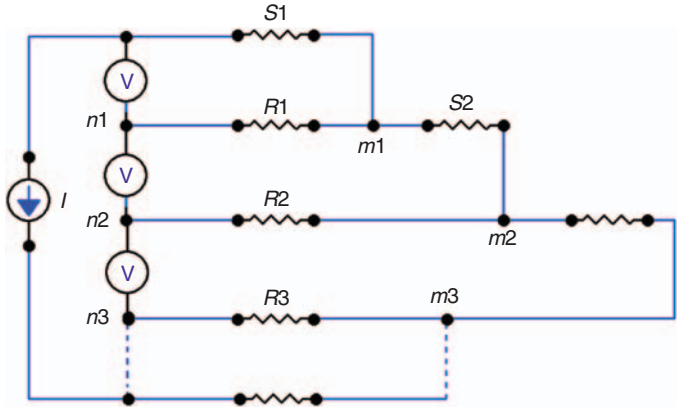

Figure 7 ULKG electrical model and acquisition technique

3. Sensing properties

In the literature, static piezo-resistive properties of CE sensors are described by using percolation theory (Taya *et al*., 1998). What is widely neglected is the behaviour of the electrical resistance of CEs during the transient time and other non-linear phenomena occurring after deformation. Unfortunately, the long response time and non-linear transduction phenomena require a complex treatment of signals, which will be described in the present section. CE sensors have been characterized in all their relevant figures of merit. The main aim has been to determine the relation between the electrical resistance $R(t)$ of a treated fabric sample and its actual length $l(t)$. An analysis of the thermal transduction properties and aging of the fabric has been executed in a previous work (Scilingo *et al*., 2003).

3.1 Static sensor characterization

In terms of quasi-static characterization, a sample of 5 mm in width (Figure 1) shows an unstretched electrical resistance of about 1 kΩ/cm, and its gauge factor $[GF = (l(R - R_0))/R(l - l_0))]$ is about 2.8, where R is the electrical resistance, l is the actual length, R_0 is the electrical resistance corresponding to l_0, which represents the rest length of the specimen). The temperature coefficient ratio is $0.08\,K^{-1}$. Capacity effects shown by the sample are negligible up to 100 MHz.

3.2 Dynamic characterization

Two different issues had to be addressed to use CE as strain sensors. The first concerns the duration of the transient time, which occurs in the relaxation phase after a deformation. It is obvious that these physical systems cannot describe human movements without signal processing devoted to compensate for the slowness of this phenomenon. Moreover, electrical response of the analysed specimen shows some non-linear phenomena, which are not negligible under certain working conditions, in particular when fast deformations are applied.

The typical electrical behaviour of these systems, when deformations in length are applied, will be described. All the remarks pointed out in our analysis will lead to the formulation of a mathematical model, which approximates the sensor electrical response. The obtained model will be used to implement an algorithm devoted to the system regulation, which consents the sensor length reconstruction in real time. Finally, two simplified and faster versions of this methodology will be presented and applied in posture reconstruction.

The analysis of the electrical trend of CE sensors, when deformations are applied, has been performed by using a system realized in our laboratories, which can provide controlled deformations and at the same time can acquire the resistance value assumed by the specimen. A description of this instrumentation and its performances

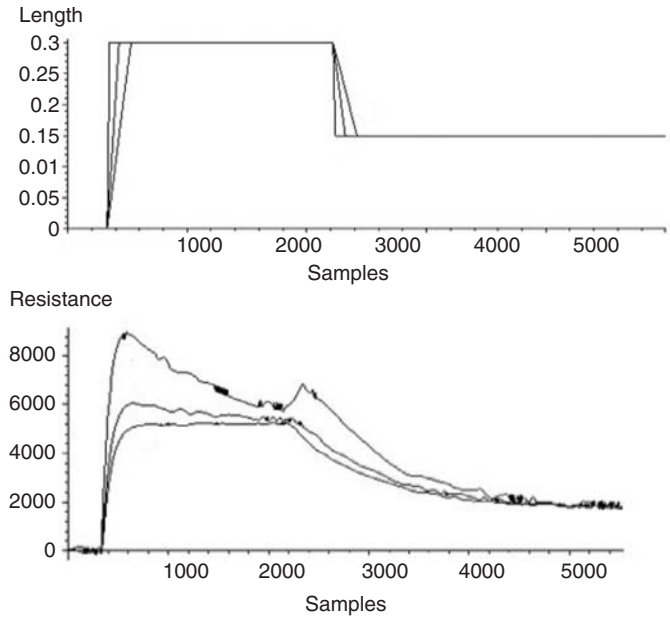

Figure 8 Response of a CE sensor excited by trapezoidal ramps in deformation

can be found in Scilingo *et al*. (2003). By using this device, several deformations, which differ in their shapes versus time, amplitudes and velocities have been applied to CE specimens. Figure 8 shows the output of a sample stretched with trapezoidal ramps in deformation having different velocities $\dot{l}(t)$ (where $l(t)$ is the length of the sample). The main remarks on sensor behaviour are summarized in the following:

- Both in case of deformations that increase the length of the specimen and in case of deformations that reduce it, two local maxima greater than both the starting value and than the regime value occur.
- If the relationship between $R(t)$ and $l(t)$ were linear, one of the extreme described in the previous point would be a minimum.
- The height of the overshoot peaks increases with the rate of strain ($\dot{l}(t)$).
- The relaxing transient time, which lasts up to several minutes, is too long to code human movements suitably.
- By using experimental data, we have verified that when the specimen is motionless, ie, $\dot{l}(t) = 0$ the signal deriving from the sensor is representable by a linear combination of exponential functions:

$$Y(t) = c_0 + c_1 e^{-\omega_1 t} + \cdots + c_p e^{-\omega_p t} \tag{2}$$

where values ω_i do not depend on the amplitude and velocity for a wide range of the solicitation previously applied (0–50% of the rest length and 0–0.1 m/s),

but they vary only according to the shape and the dimensions of the specimen and on the percentages of the components in the mixture used to realize it (Lorussi, 2003).

Non-linearity in the functional which relates $R(t)$ and $l(t)$ suggested us to choose an approximation containing a quadratic term in the strain velocity ($\dot{l}(t)$). Let us consider:

$$g(t) = a_1 l(t) + a_2 \dot{l}(t) + a_3 \dot{l}(t)^2 \tag{3}$$

where a_1, a_2 and a_3 are three non-zero real numbers. By considering that $g(t)$ has the input function of the differential linear system

$$\dot{\mathbf{x}}(t) = \mathbf{A} \cdot \mathbf{x}(t) + \begin{bmatrix} 0 \\ \vdots \\ g(t) \end{bmatrix} \tag{4}$$

where $\mathbf{x} = [\, R \quad \dot{R} \quad \ddot{R} \quad \ldots]^T$, we have obtained encouraging results in signal modelling (Lorussi, 2003). In particular, we have approximated the sensor behaviour as the solution of a second-order linear system based on Equation (4):

$$\begin{bmatrix} \dot{R} \\ \ddot{R} \end{bmatrix} = e^{\mathbf{A}(t-t_0)} \cdot \begin{bmatrix} R_0 \\ \dot{R}_0 \end{bmatrix} + \int_{t_0}^{t} e^{\mathbf{A}(t-\tau)} \cdot \begin{bmatrix} 0 \\ g(\tau) \end{bmatrix} \mathrm{d}\tau \tag{5}$$

with

$$\mathbf{A} = \begin{bmatrix} 0 & 1 \\ -\omega_1 \cdot \omega_2 & -(\omega_1 + \omega_2) \end{bmatrix} \tag{6}$$

where ω_1 and ω_2 are the two poles of the linear system (5). This relation provides an obvious method to calculate $g(t)$; since Equation (4) contains only $R(t)$ and its derivatives, it is simple to determine the value of $g(t)$. So to obtain $l(t)$ in real time, it is necessary to integrate the differential Equation (3) (in which the three parameters a_1, a_2 and a_3 have been identified through the values of peaks excursions in the responses of the sensor). Unfortunately, Equation (3) cannot be generally integrated when $g(t)$ is unknown and its solution $l(t)$ has to be numerically computed. This is not a simple issue because the acquired data are affected by noise and sampling errors. Good results have been obtained offline by using a wide digital filtering (Lorussi, 2003). Next developments in our study will be aimed at implementing the specimen length detection in real time during a motion. Conversely, the problem has been already addressed when the system is motionless, ie, $\dot{l}(t) = 0$ and $g(t) = a_1 \cdot l(t)$, and will be treated in the next section.

3.3 System regulation

After a mechanical solicitation, CE sensor resistance changes according to Equation (2). Unfortunately, the values determined for ω_i and the resulting transient

time do not allow directly employment of the acquired signals for our applications. On the other hand, by using Equation (2) it has been possible to predict the coefficient c_i (and in particular c_0, which represents the final value of the signal) early with respect to the transient time duration. Since the pole values are invariant with the deformation, in order to apply relation (2), they have to be calculated only once, during the system parameter identification. If the ω_i are known only the c_i remain undetermined and have to be online computed after each deformation. The parameter identification is realized by an algorithm, which performs a minimization of the quantity

$$J = \sum_{j=1}^{j=k} \left(y_j - (c_0 + c_1 e^{-\omega_1 t_j} + \cdots + c_p e^{-\omega_p t_j}) \right)^2 \tag{7}$$

over a lattice L, which spans the variables $c_0 \ldots c_p$, $\omega_1 \ldots \omega_p$ and where y is a k-dimensional vector containing the acquired data during the transient time after a solicitation. The choice of k is governed by the noise that affects the signal and the precision in the parameters identification increases with it. Practically, this procedure is repeated several times and the values obtained for the ω_i are the average responses evaluated on all the trials. Figure 9 shows a two-pole regression on

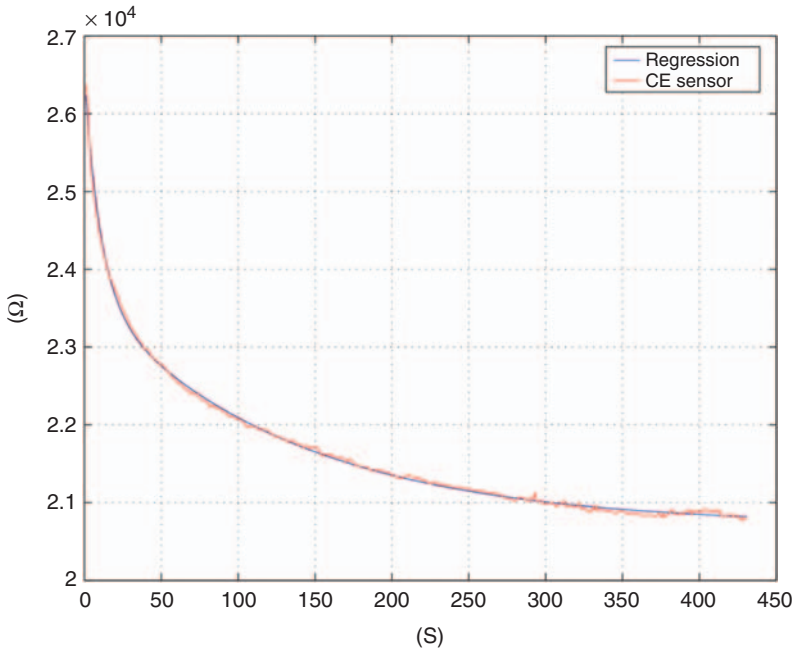

Figure 9 Two-pole regression on a CE sensors response obtained where Equation (2) holds

a CE sensor response. When we have determined the pole values, after each solicitation, coefficients $c_0 \ldots c_p$ have to be re-calculated to return the regime value and the related sensor length. We have developed two different procedures to calculate them.

3.3.1 Derivative-based regime value reconstruction algorithm: The first procedure consists of considering the iterate p derivatives of function (2) with respect to t. If $k \geq p$, the set of these equations evaluated on k samples and compared with the numerical derivatives of the signal stored in vector y constitutes a well-dimensioned linear system in the variables c_i, which can be calculated with low computational cost (as shown in Equation (11) with $p=2$ and $k=2$). This methodology, however, presents a serious disadvantage. The computation of the numerical derivatives of the signal y is invalidated by the noise that affects the signal. Moreover, the sampling noise relating to the analogue–digital (AD) converter in the electronic acquisition system is amplified by its derivation. Practically, this strategy is inapplicable in this form. Results remarkably improve if the derivation of the signals deriving from sensors is made via analogical differentiators. Let us consider an example dealing with the two-pole approximation of the CE sensor behaviour during its transient time (Equation (2) with $p=2$)

$$Y(t) = c_0 + c_1 e^{-\omega_1 t} + c_2 e^{-\omega_2 t} \tag{8}$$

and let us calculate the first and second derivative of Equation (8). Our goal is to eliminate exponential terms by using a linear combination of $Y(t)$ and its first and second derivative:

$$a\,Y(t) + b\,\dot{Y}(t) + c\,\ddot{Y}(t) \tag{9}$$

By setting the linear combination of Equation (9) equal to c_0, it is possible to predict the regime value (when the specimen is motion less). Thus, we obtain:

$$\begin{aligned} &a\left(c_0 + c_1 e^{-\omega_1 t} + c_2 e^{-\omega_2 t}\right) + b\left(-c_1\omega_1 e^{-\omega_1 t} - c_2\omega_2 e^{-\omega_2 t}\right) + \cdots \\ &\cdots + c\left(c_1\omega_1^2 e^{-\omega_1 t} + c_2\omega_2^2 e^{-\omega_2 t}\right) = c_0 \end{aligned} \tag{10}$$

From Equation (10), we extract the following system:

$$\begin{cases} ac_0 = c_0 \\ a - b\omega_1 + c\omega_1^2 = 0 \\ a - b\omega_2 + c\omega_2^2 = 0 \end{cases} \tag{11}$$

The system of expression (11) satisfies Rouche–Capelli's theorem and its solution is univocally determined.

$$\begin{cases} a = 1 \\ b = \dfrac{1 + c\omega_1^2}{\omega_1} \\ c = \dfrac{\omega_2 - \omega}{\omega_1\omega_2^2 - \omega_1^2\omega_2} \end{cases} \tag{12}$$

By substituting these a, b and c in expression (9), we directly obtain the final value of the sensor resistance.

By summarizing, the knowledge of the sensor pole values and a preliminarily calculation of the coefficients of the linear combination of relation (10) permit us to determine the final value of the sensor resistance in advance with respect to the long relaxation time. Before employing a sensor, it is necessary to perform its calibration in order to evaluate the poles and estimate the coefficients a, b and c.

The detection of the regime value has been obtained via hardware (Figure 10) by designing a dedicated electronic device. The CE sensor output provides three different blocks. In the first one it is amplified with a gain a, in the second one it is differentiated and amplified by b and the third one it is differentiated twice and multiplied by c. After the amplification, the three signals are added, and the result is the regime value of the relaxing response. In Figure 11, the output of the scheme described above is reported and compared with the sensor response. The sensor was solicited by a sequence of three square-waves having different length and amplitude. It is clear from the same figure that the treated response quickly predicts the regime value of the sensor resistance value.

This solution addresses the problems introduced by the AD conversion noise. In addition, a wide low-pass filtering is needed (in fact, the 50-Hz network noise, always present in normal condition, is amplified by its second derivative of a rate

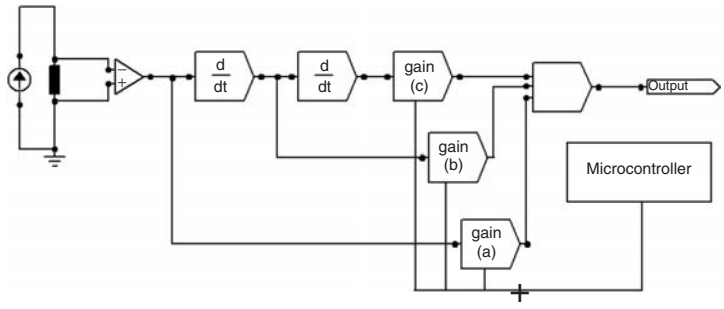

Figure 10 The block diagram of the system for detecting the final value of the response of the sensor submitted to a stepwise stretching

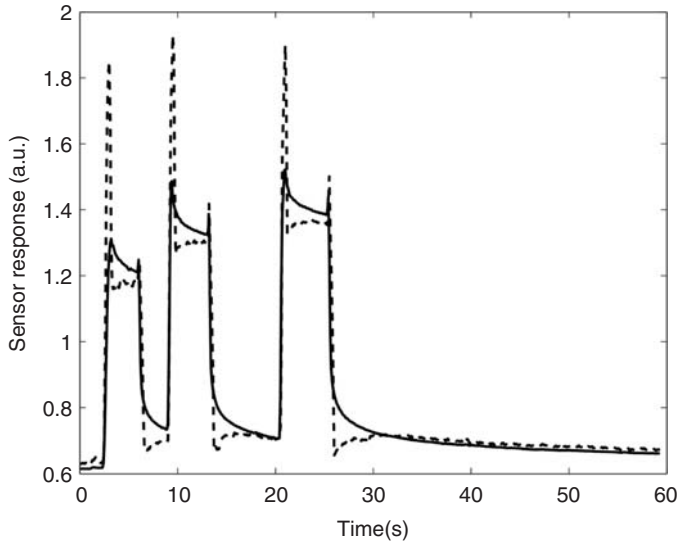

Figure 11 Comparison between the sensor response (continuous line) and the treated output (dashed line)

equal to 2500). This last operation generates a significant delay. Hence, the use of the presented strategy requires an arrangement between signal quality and an effective final value prediction. Another disadvantage of the described technique is the increase of the electronic acquisition system dimension because of the components necessary to implement differentiators and the simultaneous acquisition of signals and their derivatives, which exploits the number of the AD converter channels (Tognetti *et al.*, 2004).

3.3.2 Integral-based regime value reconstruction algorithm: To address this issue and eliminate noise deriving from the presence of high impedance connecting wires and from the electrical network (Tognetti *et al.*, 2004), we have developed an algorithm based on iterate integrations of Equation (2). Coefficients $\{c_i\}_{i=0...p}$ are in this case the solution of an over-dimensioned linear system $n \times p$, obtained by integrating Equation (2) n times on the interval $[t_0, t_k]$. It is easy to prove that the system obtained is consistent for $n \geq p$ and $k \geq p$ by computing the Jacobian matrix of the system in its parametrical form. The choice of $n > p$ produces a wide filtering of signals while the coefficients are calculated. A further stabilization is related to the integration on the entire interval where Equation (2) holds, by collecting all the information previously stored. No particular disadvantages arise from these methods. All the calculation is digitally computed with neither increasing the dimension of the electronic acquisition system nor introducing or amplifying further noise. The only cunning necessary consists of detecting each movement because Equation (2) holds when the

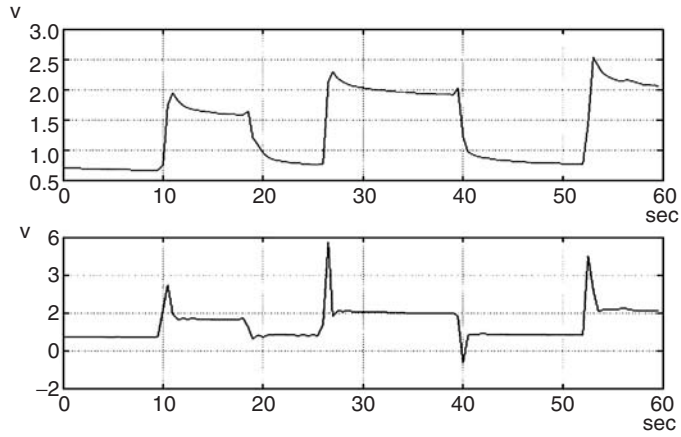

Figure 12 Output of a CE sensor (voltage versus time) with three different deformation steps imposed (above) and treated signal (below). The transient time has been reduced

specimen is motionless only, and the numerical integration has to be reset after each solicitation. Results are reported in Figure 12.

4. Applications: posture and gesture recognition

CE sensors distributed over a kinaesthetic garment can detect local deformations on the fabric during the user movement. Algorithms for mapping these raw sensor data into user kinematic configurations have to be formulated in order to adopt presented sensing systems in biomechanical reconstruction.

4.1 Posture and gesture detection

In order to explain how posture detection can be executed by using a kinaesthetic garment, some remarks are necessary. First, to define a posture formally, it is necessary to develop a geometrical model of the kinematic chain under study (Section 5.1). This can be done by fixing a certain number of Cartesian frames, one for each DOF considered and by relating them with the segments that compose the kinematic chain. A kinematic configuration consists of the set of the mutual positions of these Cartesian frames. When a kinaesthetic garment worn by a user holds a certain posture described by its geometrical model, the set of sensors assumes a certain value strictly related to it. If the number of sensors is large enough and if the sensor locations are adequate, then the values presented by them uniquely characterize the considered posture. Considering the ULKG (or any other kinaesthetic garment presented in Section 2.2) and let $S \subset \mathbf{R}^k$ be the sensor space, ie, the vectorial space whose elements contain the

values presented by sensors and where k is equal to the sensor number in the ULKG. Let $\Theta \subset \mathbf{R}^n$ be the space containing the kinematic configurations, ie, the space of the Lagrangian co-ordinates that define the mutual segment positions in an upper limb kinematic model, where n is equal to the number of DOFs considered. To execute a reconstruction of the kinematic configuration, by knowing the sensor status, a function **F**, which maps Θ into S, has to be defined.

We have implemented **F** both by a clusterization of the space S via a clustering norm technique into the space Θ (Section 4.2.1) and by the interpolation of the discrete map produced by the clusterization (Section 4.2.2). The first solution has been applied by using the norm

$$\delta = \sqrt{\sum_{i=1}^{i=k} |s_i - S_i|} \tag{13}$$

as a clustering function, where $\mathbf{S} \in S$ is a k-dimensional vector, which represents a centre of the clusterization lattice and $\mathbf{s} \in S$ is a k-dimensional vector representing the real values assumed by the sensors. Each point $\mathbf{S}^*$, whose distance from a certain point of the lattice $\mathbf{S}^*$ is less than a previously fixed threshold $\boldsymbol{\varepsilon}$ is related to the value that the map assumes in $\mathbf{S}^*$. The values the function holds in the points of the clusterization lattice is experimentally acquired. The other implementation of **F** is described Section 4.2.2 (Lorussi *et al*., 2004).

4.2 Kinaesthetic garments working modes

4.2.1 Sensorized garments as posture and movement recorders: By using the kinaesthetic garments presented in this work, it is possible to detect whether two postures are the same with a certain tolerance, and it is also possible to record a certain set of postures coded by the status of the sensors. In the same way, movements can be recorded as transition from a posture to another one, and they are coded by the evolution of the sensor values. In particular, we have tested this capability on a set of functional relevant postures both for the ULKG and for the sensing glove.

ULKG: This garment showed good capabilities of repeatability, even if it is removed and re-worn. *Ad-hoc* software devoted to recognize recorded postures has been developed (Figure 13). The software is able to:

- record a set of defined postures in a calibration phase;
- recognize the recorded postures during the user's movements; and
- display the movement by using animations in a 3D environment.

In the calibration phase, the user who wears the ULKG holds a set of positions $\boldsymbol{\theta}_i$ ($i = 1 \ldots p$, where p is the number of postures to be recorded) and the sensor status $\mathbf{s}_i^c$

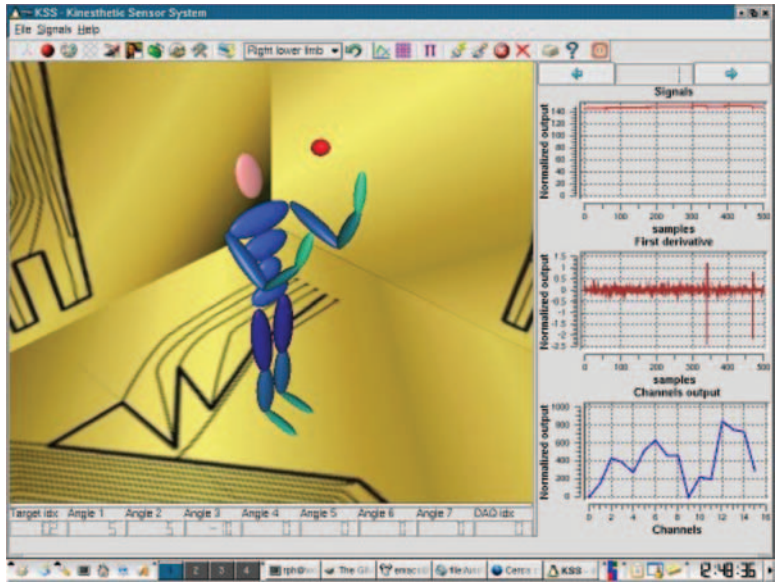

Figure 13 The developed software package for ULKG

is acquired and stored in the $k \times p$ calibration matrix $\hat{\mathbf{C}}$

$$\hat{\mathbf{C}} = \left[\mathbf{s}_1^c \ldots \mathbf{s}_i^c \ldots \mathbf{s}_p^c\right]$$

In the recognition phase, while the user moves the upper limb, the kinematic configuration is detected by acquiring the sensor outputs $\mathbf{s}$ and by comparing them with the p columns of the calibration matrix. If the distance induced by the norm expressed in Equation (13) between the actual sensor values and a column of the matrix is smaller than a certain threshold, the ULKG returns the position related to the selected column. In this application, it is not necessary to map the entire space of the sensor values into the configuration space, so any other norm, instead of the one defined by Equation (13), can be used. The system has also been tested by implementing the Euclidean norm of expression (14), and it has performed the same results.

$$\delta = \sqrt{\sum_{i=1}^{i=k} (s_i - S_i)^2} \tag{14}$$

When a posture is recognized, visualization software performs an animation (Section 5) from the old position to the actual one.

Sensing glove: Using the sensorized glove, we have recorded the status of the sensors in a set of relevant kinematic configuration for the hand: the eight

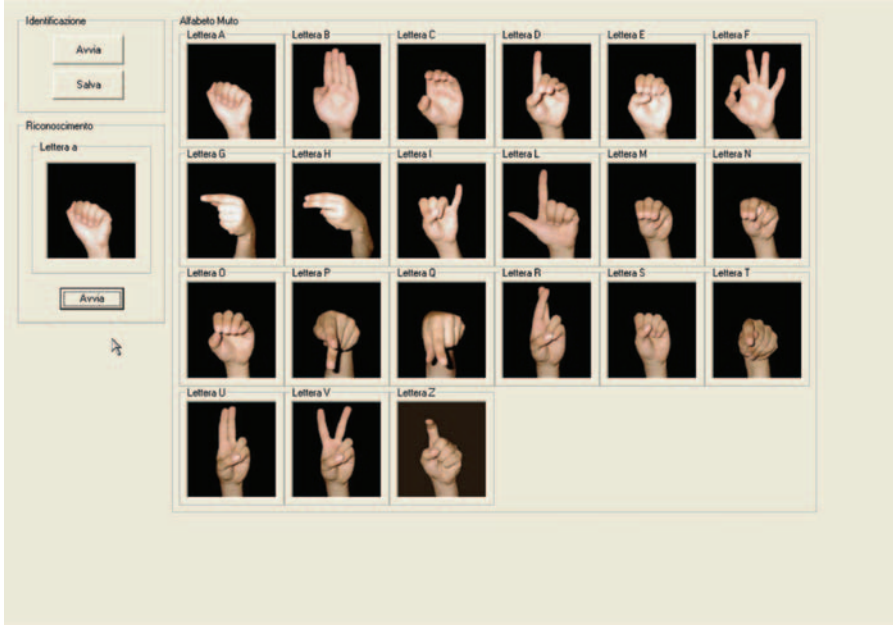

Figure 14 American Sign Language recognition using the sensing glove

'fundamental' hand grips and the signs of the American Sign Language have been considered. By using the approach employed for the UKLG, *ad-hoc* software devoted to recognize recorded postures has been developed (Figure 14).

4.2.2 Kinaesthetic garments as posture detector: According to the previous section, kinaesthetic garments are able to record the sensor status in a finite number of positions in the configuration space. These data can be related to corresponding positions to define a discrete map between two subsets of the two spaces. An example of this map is the function that relates the centres of the clusters in the lattice introduced in Section 4.2.1 with the corresponding geometrical configurations. If the set of the points considered in the configuration space satisfies some particular requirements (Lorussi *et al.*, 2004), this map can be extended by interpolation techniques to all the configuration space.

System identification: The problem can be formalized as follows. Let us assume Θ as a fixed state space (the posture space, described by a set of frames assigned and by their mutual co-ordinate transformations). In order to detect a posture, it is necessary to relate the elements of Θ to the sensor configurations that span the space S of sensor values. Let us assume the set of sensors is able to detect a subject's posture variation and there exists an invertible function **F** that maps the posture space into S.

As a consequence, the image of Θ through $\mathbf{F}$ is a subset of S which has the same dimension of Θ. Therefore, the inverse of $\mathbf{F}$ can be used to infer a posture ($\boldsymbol{\theta}$) from the sensor status ($\mathbf{s}$)

$$\boldsymbol{\theta} = \mathbf{F}^{\dagger} \cdot \mathbf{s} \tag{15}$$

where $\mathbf{F}^{\dagger}$ is the pseudo inverse of $\mathbf{F}$ (in our application, because of redundancy, the S space dimension is usually greater then the Θ one).

The construction of $\mathbf{F}$, or 'system identification', is the crucial point in our method and it is important from several points of view. It is worth pointing out that this phase is not a single sensor calibration, but it is a real identification of the entire system. In fact, the sensor location is not exactly known, as an example, in case of variability of the subject's body structure. This redundancy concept has been expressed also in Section 2.2.2. However, by adopting the described approach, neither the knowledge of the sensor locations nor the relation between the sensor size and the electrical resistance is essential. To clarify this point, some remarks are necessary. The adherence of a kinaesthetic garment to its wearer gives rise to an intrinsic cross-talk phenomenon. This, instead of being an inconvenience, is instrumental to the method we have developed, and it ensures the possibility of posture reconstruction without knowing each single sensor location. The identification not only concerns the set of sensors, but the body structure of the subject is also considered. In this case, the same sensing garment can be used to detect the posture of different subjects with the prescribed accuracy by shifting the body variability on $\mathbf{F}$.

A crucial point in the building of $\mathbf{F}$ is the choice of a parameterization for Θ. The basic idea is to perform the Θ parameterization by using a conventional measurement system. For example, in our experiments with the ULKG we used a set of electro-goniometers produced by Biometrics Ltd. Figure 15 shows the sensing glove endowed with the set of electro-goniometers during the identification phase. The parameterization is simultaneously performed together with the construction of $\mathbf{F}$. This can be done by relating information coming from the conventional measurement system to the sensor status. In this way, a certain number of configurations in the articulation workspace is mapped into sensor status. This point concerns the construction of a restriction of $\mathbf{F}$ over a lattice $L' \subset \Theta(\mathbf{F}|_{L'})$.

$$\begin{array}{ccc} S & \xleftarrow{\mathbf{F}} & \Theta \\ \uparrow & \mathbf{F}|_{L'} & \cup \\ \leftarrow & & L' \end{array}$$

The next step is to expand the knowledge of $\mathbf{F}|_{L'}$ defined by its restriction to all Θ, obtaining $\mathbf{F}$. This is a problem of multivariate interpolation. A piecewise linear interpolation (Veldhuizen, 1998) technique based on the decomposition of Θ into a lattice compounded by hyper-tetrahedra is explained in Lorussi *et al*. (2004). The choice of the PL interpolation is related to the necessity to invert $\mathbf{F}$. PL functions

Figure 15 The sensing glove and the electro-goniometers during the calibration phase

Table 1 Wrist range of motion

	Flexion–extension	Abduction–adduction
Min	−80°	−30°
Max	80°	30°

are linear applications and they are invertible with low computational cost. If the set of configurations is coded by a parameterization and if $\mathbf{F}^{\dagger}$ is available, the posture of a user can be determined with a precision depending on the interpolation used. The procedure for the determination of the position only consists of the detection of the piece of $\mathbf{F}^{\dagger}$ which holds for the particular sensor values $\mathbf{s}$ and in multiplying $\mathbf{F}^{\dagger}\cdot\mathbf{s}$.

Interpolation technique and inversion: To better explain the PL interpolation technique, a reconstruction of the two wrist DOFs using five sensors of the ULKG is reported as an example. An average wrist workspace (Kapandji, 2004) is reported in Table 1.

The wrist workspace has been divided into a fixed number of rectangles (hyper-cubes of second-order $\mathbf{I}_2^i$). A step of 40° for the flexion–extension angle and a step of 15° for the abduction–adduction angle have been used. Therefore, we obtain 16 hyper-cubes of order 2 (rectangles with dimension 40° and 15°) whose union covers all the wrist configuration space. This partition of the configuration space Θ is shown in Figure 16. Each rectangle has been divided in two triangles (hyper-tetrahedra

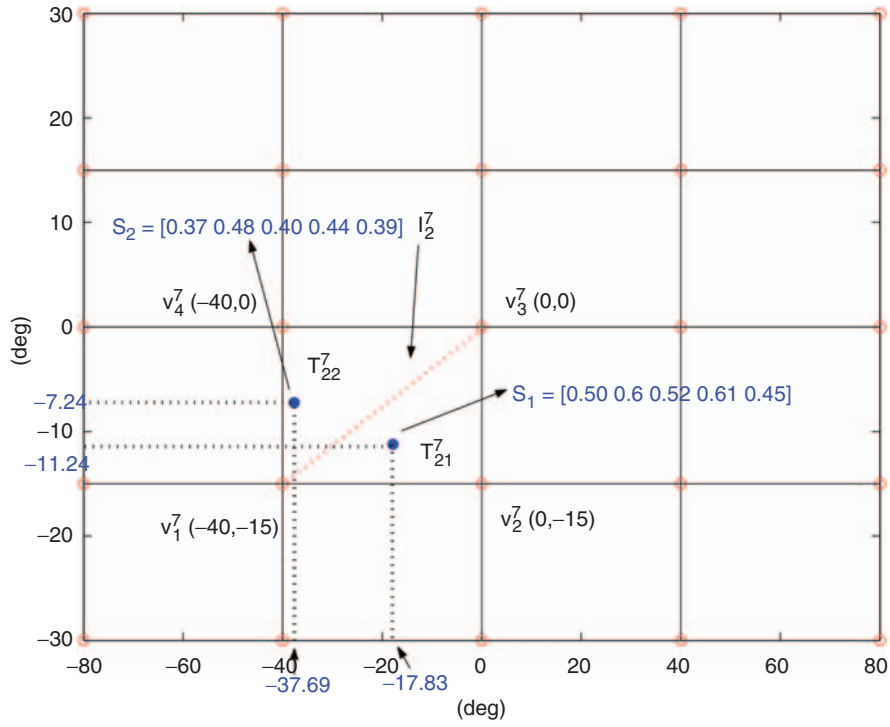

Figure 16 Partition of the configuration space for the wrist articulation

of order 2). Figure 16, which has been reported as an example, represents the hyper-cube $\mathbf{I}_2^7$, which has been divided into two triangles ($\mathbf{T}_{21}^7$ and $\mathbf{T}_{22}^7$) whose vertices are:

$$\mathbf{T}_{21}^7 = \begin{bmatrix} v_1^7 & v_2^7 & v_3^7 \\ (-40;-15) & (0;-15) & (0;0) \end{bmatrix} \tag{16}$$

$$\mathbf{T}_{22}^7 = \begin{bmatrix} & v_4^7 & \\ (-40;-15) & (-40;0) & (0;0) \end{bmatrix} \tag{17}$$

In all, we have:

- 16 hyper-cubes $\mathbf{I}_2^i$;
- 32 hyper-tetrahedra $\mathbf{T}_{2j}^i$;
- 25 calibration points, which are the vertices of the hyper-cubes, represented by the empty circles in Figure 16.

In the following, the exact sequence to effectively obtain **F** will be reported. First, the sensor status corresponding to each rectangle's vertex is acquired. The rectangles'

vertices are determined by using the external measurement system (electrogoniometers). This phase exactly corresponds to the construction of the restriction of **F** on $L' \subset \Theta$ ($(\mathbf{F}|_{L'})$, Section 4.2.2).

Once again, considering $\mathbf{I}_2^7$, we have

$$v_1^7 = (-40; -15) \rightarrow \mathbf{s}_{v_1^7} = [0.406 \quad 0.510 \quad 0.429 \quad 0.483 \quad 0.430] \tag{18}$$

$$v_2^7 = (0; -15) \rightarrow \mathbf{s}_{v_2^7} = [0.612 \quad 0.543 \quad 0.440 \quad 0.667 \quad 0.399] \tag{19}$$

$$v_3^7 = (0; 0) \rightarrow \mathbf{s}_{v_3^7} = [0.584 \quad 0.746 \quad 0.568 \quad 0.760 \quad 0.699] \tag{20}$$

$$v_4^7 = (-40; 0) \rightarrow \mathbf{s}_{v_4^7} = [0.312 \quad 0.413 \quad 0.351 \quad 0.353 \quad 0.321] \tag{21}$$

where $[\mathbf{s}_{v_1^7} \ldots \mathbf{s}_{v_4^7}]$ is the sensor status (with normalized values) estimated in the vertices of $\mathbf{I}_2^7$. Then, for each triangle of the partition ($\mathbf{T}_{2j}^i \quad i = 1 \ldots 16 \quad j = 1 \ldots 2$) the interpolating function $\mathbf{F}|_{T_{2j}^i}$ ($\mathbf{R}^2 \rightarrow \mathbf{R}^5$) has been calculated, by determining the equation of the plane passing for the triangle vertices and their corresponding sensor values. By considering $\mathbf{T}_{21}^7$, and fixing x as the flexion–extension axis, y as the abduction–adduction axis and z_i ($i = 1 \ldots 5$) as the axis of the interpolated values, we obtain:

$$\mathbf{z} = \begin{bmatrix} z_1 \\ z_2 \\ z_3 \\ z_4 \\ z_5 \end{bmatrix} = \mathbf{F}\Big|_{\mathbf{T}_{21}^7} \begin{bmatrix} 0.005150x & -0.001867y & +0.584000 \\ 0.000825x & +0.013533y & +0.746000 \\ 0.000275x & +0.008533y & +0.568000 \\ 0.004600x & +0.0062000y & +0.760000 \\ -0.000775x & +0.020000y & +0.699000 \end{bmatrix} \tag{22}$$

which, in a compact form can be written as:

$$\underset{\mathbf{z}}{\begin{bmatrix} z_1 \\ z_2 \\ z_3 \\ z_4 \\ z_5 \end{bmatrix}} - \underset{\mathbf{z}'\big|_{\mathbf{T}_{21}^7}}{\begin{bmatrix} 0.584000 \\ 0.746000 \\ 0.568000 \\ 0.760000 \\ 0.699000 \end{bmatrix}} = \underset{\mathbf{F}'\big|_{\mathbf{T}_{21}^7}}{\begin{bmatrix} 0.005150 & -0.001867 \\ 0.000825 & +0.013533\mathrm{y} \\ 0.000275 & +0.008533\mathrm{y} \\ 0.004600 & +0.0062000 \\ -0.000775 & +0.020000 \end{bmatrix}} \cdot \begin{bmatrix} x \\ y \end{bmatrix}$$

$$\mathbf{z} - \mathbf{z}'\Big|_{\mathbf{T}_{21}^7} = \mathbf{F}'\Big|_{\mathbf{T}_{21}^7} \begin{bmatrix} x \\ y \end{bmatrix}$$

In a general case, we have:

$$\mathbf{z} - \mathbf{z}'\big|_{\mathbf{T}_{2j}^{i}} = \mathbf{F}'\big|_{\mathbf{T}_{2j}^{i}} \begin{bmatrix} x \\ y \end{bmatrix} \tag{23}$$

The union of all the interpolating function ($\mathbf{F}|_{\mathbf{T}_{2j}^{i}}.$) is the desired function $\mathbf{F}$ of Section 4.2.2.

In the detection phase, when a sensors status $\mathbf{s}$ holds, the inverse function of $\mathbf{F}$ has to be computed and then applied to $\mathbf{s}$. In our example, since the sensor status $\mathbf{s}$ is related to a certain unknown wrist kinematic configuration, first the correct piece ($\mathbf{F}|_{\mathbf{T}_{2j}^{i}}.$) compounding $\mathbf{F}$ has to be determined and its pseudo-inverse ($\mathbf{F}|_{\mathbf{T}_{2j}^{i}}\dagger$) has to be applied to s:

$$\begin{aligned} \begin{bmatrix} x \\ y \end{bmatrix} &= \left(\left(\mathbf{F}'\big|_{\mathbf{T}_{2j}^{i}}^{T} \cdot \mathbf{F}'\big|_{\mathbf{T}_{2j}^{i}} \right)^{-1} \cdot \mathbf{F}'\big|_{\mathbf{T}_{2j}^{i}}{}^{T} \right) \cdot \left(\mathbf{s} - \mathbf{z}'\big|_{\mathbf{T}_{2j}^{i}} \right) \\ \begin{bmatrix} x \\ y \end{bmatrix} &= \left(\mathbf{F}'\big|_{\mathbf{T}_{2j}^{i}} \right)^{\dagger} \cdot \left(\mathbf{s} - \mathbf{z}'\big|_{\mathbf{T}_{2j}^{i}} \right) \end{aligned} \tag{24}$$

Considering the example in Figure 16, we have

$$\mathbf{S}_1 = \begin{bmatrix} 0.5 \\ 0.6 \\ 0.52 \\ 0.61 \\ 0.45 \end{bmatrix} \tag{25}$$

According to the sensors status it is possible to find $\mathbf{T}_{21}^{7}$ containing (x, y). By considering (24)

$$\begin{aligned} \begin{bmatrix} x \\ y \end{bmatrix} &= \mathbf{F}'\big|_{\mathbf{T}_{21}^{7}}^{\dagger} \cdot \left(\mathbf{s}_1 - \mathbf{z}'\big|_{\mathbf{T}_{21}^{7}} \right) = \\ &= \begin{bmatrix} 106.834 & 10.219 & 1.401 & 91.502 & -25.907 \\ -5.265 & 19.150 & 12.193 & 6.665 & 29.285 \end{bmatrix} \cdot \left(\begin{bmatrix} 0.5 \\ 0.6 \\ 0.52 \\ 0.61 \\ 0.45 \end{bmatrix} - \begin{bmatrix} 0.584 \\ 0.746 \\ 0.568 \\ 0.760 \\ 0.699 \end{bmatrix} \right) \\ &= \begin{bmatrix} -17.83 \\ -11.24 \end{bmatrix} \end{aligned} \tag{26}$$

Once again considering the example of Figure 16 and having as input $\mathbf{s}_2$

$$\mathbf{s}_2 = \begin{bmatrix} 0.37 \\ 0.48 \\ 0.40 \\ 0.44 \\ 0.39 \end{bmatrix}$$

According to the sensors status it is possible to find $\mathbf{T}_{22}^{7}$ containing (x, y) and by considering the appropriate pseudo-inverse we obtain

$$\begin{aligned} \begin{bmatrix} x \\ y \end{bmatrix} &= \mathbf{F}'\big|^{\dagger}_{\mathbf{T}_{22}^{7}} \cdot (\mathbf{s}_2 - \mathbf{z}'\big|_{\mathbf{T}_{22}^{7}}) = \\ &= \begin{bmatrix} -325.092 & 295.636 & -374.727 & -77.708 & 378.098 \\ -414.260 & 325.186 & -468.937 & -129.392 & 420.142 \end{bmatrix} \cdot \left(\begin{bmatrix} 0.37 \\ 0.48 \\ 0.40 \\ 0.44 \\ 0.39 \end{bmatrix} - \begin{bmatrix} 0.584 \\ 0.746 \\ 0.568 \\ 0.760 \\ 0.699 \end{bmatrix} \right) \\ &= \begin{bmatrix} -37.69 \\ -7.24 \end{bmatrix} \end{aligned} \tag{27}$$

The detected angles $\boldsymbol{\theta}_1 = [-17.63 \ -11.24]$ and $\boldsymbol{\theta}_2 = [-27.69 \ -7.24]$ are represented by the two solid circles in Figure 16.

It is worth the effort to point out that the presented method is time-consuming only when it calculates the 32 pseudo-inverses $\mathbf{F}|^{\dagger}_{\mathbf{T}_{2j}^{i}}$, but this calculation is computed only once.

5. Kinematic chain control

Kinaesthetic garments presented in Section 2.2 can be used to acquire data about posture, gesture and movement, and can be applied in many control tasks in biomechanics and robotics. In the present section, we describe the realization of a dedicated software where acquired data from the ULKG are used to drive a kinematic model of the human upper limb in an interactive 3D environment.

5.1 Kinematic modelling of human articulations

In many disciplines, such as biomechanics, robotics and computer graphics, geometric hierarchical structures are used in articulated body modelling for robot, human or other creatures' representations. An articulated body can be thought as a series of rigid segments connected by joints. A biological kinematic chain is an articulated body.

Table 2 Upper limb DOFs

Shoulder	Elbow	Wrist
Flexion–extension	Flexion–extension	Flexion–extension
Abduction–adduction	Pronation–supination	Abduction–adduction
Intra–extra rotation		

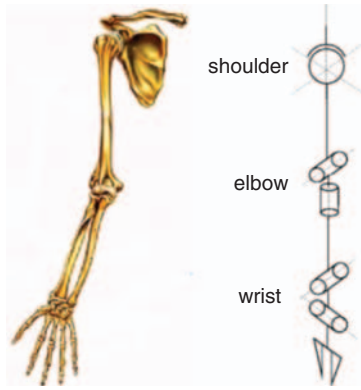

Figure 17 The upper limb model

Our developed models for human articulations use ideal joints in order to maintain a practical parameterization of movements without trivializing human motion. Regarding the upper limb, from a macroscopic point of view, a complete model would have at least 7 DOFs, corresponding to rotational movements (described by kinaesiology, and reported in Table 2). So, the gleno-humeral joint of the shoulder has been parametrized as a ball and socket joint, whereas elbow and wrist consist of two successions of two rotational joints (Figure 17). This choice has been made in order to have an intuitive kinematic reconstruction in terms of practical mathematical characterization (Euler's angles, exponential map or unit quaternion).

Finally, all kinematic models of the limbs are joined to form a virtual Avatar with human appearance, whose movements are driven by sensorized garments (Bartalesi, 2004). Mapping between sensor space S and configuration space s done by means of the algorithms already explained in Section 4. The avatar (shown in Figure 18) gives a representation of the user's movements in a virtual 3D environment.

5.2 Parameterization of rotations and animations

As clearly shown in Figure 17, the upper limb DOFs are rotational movements, each one representing an orientation between two relative reference frames. Three different

Figure 18 Animation of the avatar: transition from a recognized position to another

parameterization techniques are usually considered to describe orientations between frames:

- the Euler's angles;
- the exponential map; and
- the unit quaternion.

There is no general criterion to prefer one parameterization with respect to the others. The choice depends on the particular application. The crucial point, as a classic control problem, is the presence of singularities. Euler's angles describe the orientation of a Cartesian frame with respect to another by using three parameters, but they have two singularities. The exponential map introduces a new parameter with respect to Euler's angles but it solves only one singularity. To address both the singularities, unitary quaternions can be used. The set of quaternions H is a non-commutative algebra of hypercomplex number created in 1843 by Sir R. Hamilton. The unitary quaternions constitute a subgroup in H, which have unitary Cartesian norm. A clear summarization of their geometric properties, algebra and applications in computer graphics can be found in Shoemake (1987). We have developed our model by using both Euler's angles and unitary quaternions. This choice is related to the simplicity of the first parameterization and the low computational cost of the second. Moreover, the absence of singularities in unit quaternions permits the execution of each arbitrary trajectory in the configuration space. In other words, the possibility of executing and representing each movement allowed by the physical constraint is ensured.

5.3 Forward and inverse kinematics

Depending upon the application, there are two ways for the reconstruction of body posture: forward and inverse kinematics.

In *forward kinematics*, the 6×1 end-effector vector $\mathbf{x}$ (represented by the hand in the upper limb) is expressed by the equation:

$$\mathbf{x} = f(\boldsymbol{\theta}) \tag{28}$$

where $\mathbf{x}$ is composed by position and orientation components and $\mathbf{q}$ is the $n \times 1$ vector of Lagrangian co-ordinates for each joint in the chain (with $n = 7$ for the upper limb). In order to obtain $\boldsymbol{\theta}$, the outputs of the posture detection algorithms (Section 4) are expressed in terms of Euler's angle parameterization and they are subsequently translated in the unitary quaternion parameterization to control the avatar in the virtual environment. In Shoemake (1987), a methodology capable to perform fluid and biomimetic movements by using unitary quaternions is explained. We have applied those results to represent the transition of our geometrical model and to animate the avatar steered by the signals deriving from the sensorized garment.

On the other hand, we deal with *inverse kinematics* (IK) when the end-effector is under a well known constraint (eg, gait or grip tasks) and departing from this constrain, we have to go back to find the Lagrangian co-ordinates that ensure this position and orientation. In other words, for a given goal $\mathbf{x}$ of the end-effector, we have to solve the equation:

$$\boldsymbol{\theta} = f^{-1}(\mathbf{x}) \tag{29}$$

in the unknowns $q_i \ldots q_n$.

This is a non-linear and over-dimensioned problem. A taxonomy of algorithms for IK can be found in Tolani *et al*. (2000) and it distinguishes them from *analytical* and *numerical*. The former are those that search the complete space of solutions and the latter are those that try to converge directly to a solution by means of iterative processes. However, for kinematic chains with a number of DOF greater than 6, a criterion to solve the indetermination and eventually to resort numerical computation is needed. We have realized a numerical algorithm and tested an analytical one from the literature with very good graphical results. The idea of using IK algorithms for applications with sensorized garments arises regarding future applications. The development of smart wearable sensors (accelerometers and magnetometers for example) that could be integrated with actual sensorized garments and that will provide more accurate information about orientation and position of limbs will require this kind of computation for kinematic reconstruction.

6. Testing

In our laboratories, prototypes introduced in Section 2.2 have been tested through a series of trials in order to check the real capability of these instruments to recognize and detect gestures, postures and movements.

6.1 Kinaesthetic garments performances as posture and movement recorders

The first basic working mode, which has been tested for each system, is the kinaesthetic garment function as a posture recorder. This functionality tested the prototype hardware, the clusterization and the reconstruction algorithms described in Section 4.

6.1.1 ULKG: The ULKG has been used to record some postures for the upper limb. After having stored all the data concerning 16 different postures in the upper limb workspace, the same ones have been re-held again several times. The system has recognized the 90% of the postures recorded, and no further re-calibration has been necessary, even when the ULKG has been removed and re-worn. Postures used to test the prototype were in a generic position in the workspace.

6.1.2 Sensing glove: The glove, used as a posture recorder, requires the verification of only the hypothesis of repeatability. In the test we performed (on a set of 32 different postures, the basic grips and the signs of the American sign language – Figure 14), the glove has recognized 100% of the postures previously recorded if it was not removed from the hand, and the 98% when it has been re-worn. The percentage grows up to 100% if the wearing is re-adjusted when the first error occurs.

6.2 Kinaesthetic garments performances as posture detectors

According to Section 4.2.2, sensing prototypes have been submitted to several trials to evaluate their performance in dynamical working conditions and during the detection of unknown postures. The main proof deriving from these trials is that the kinaesthetic garments are able to reconstruct postures never recorded or held before. In each trial, the garments have been worn by a subject and a set of electro-goniometers have been positioned on him. The goniometers were adequate to detect postures and movements permitted by the joints under study and they have been used only to have a description of the movements performed. No interactions between the sensorized garments and the goniometers were allowed. During the user movements, signals deriving from the sensing garment and from the set of goniometers have been simultaneously acquired. The outputs of the sensorized garment have been processed according to Section 4.2.2 and the results obtained in terms of angles have been compared with the goniometer output. In the following figures, obtained data are shown in two different representations. The first one is a classical representation of the reconstructed angle values versus time. In the graphics included, both the sensorized garment output and the values presented by the goniometers are reported and compared. In the other representation, we have considered some planes contained in the configuration space Θ and we have plotted the trajectories performed by some joints on them, both for goniometers and for the

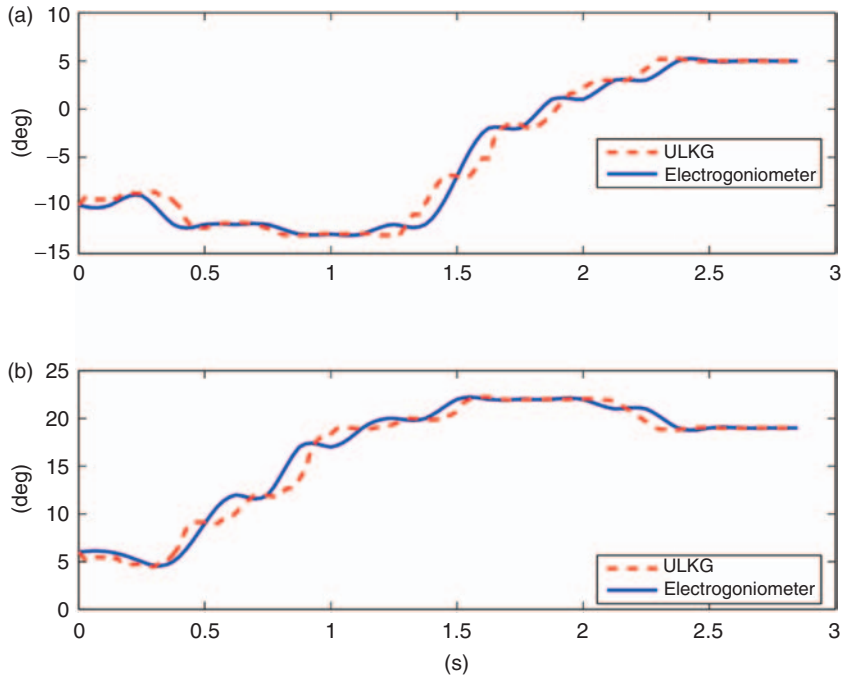

Figure 19 Flexion (a) and abduction (b) angles of the wrist versus time. The continuous line represents the goniometer output, while the dashed one represents the ULKG response

kinaesthetic garments. This presentation is very powerful to detect divergences between the two responses.

6.2.1 ULKG: In ULKG testing, the subject has been invited to perform a set of classical movements, which involve the gleno-humeral joint, the elbow and the wrist. In Figures 19 and 20, the analysis of wrist circling is reported. Figures 19(a) and 19(b) represent the flexion and abduction angles (which compound the movement) versus time. The continuous line is the goniometer output, while the dashed one represents the ULKG response. Figure 20 composes the two angle evolutions in a trajectory, which meaningfully explain the motion. Flexion is reported on the abscissa axis, while the abduction is reported on the ordinate axis. The same scheme has been adopted to report a movement for the shoulder in Figures 21 and 22. Extension is reported in Figure 21(a) (versus time) and on the y-axis of Figure 22. Conversely, Figure 21(b) and the x-axis of Figure 22 represent the evolution of the shoulder flexion. Finally, an elbow flexion is shown in Figure 23. Both shoulder rotation and elbow pronation–supination have performed qualitative results in term of sensor signal trends, but these responses have not yet been analysed because the electro-goniometers we used

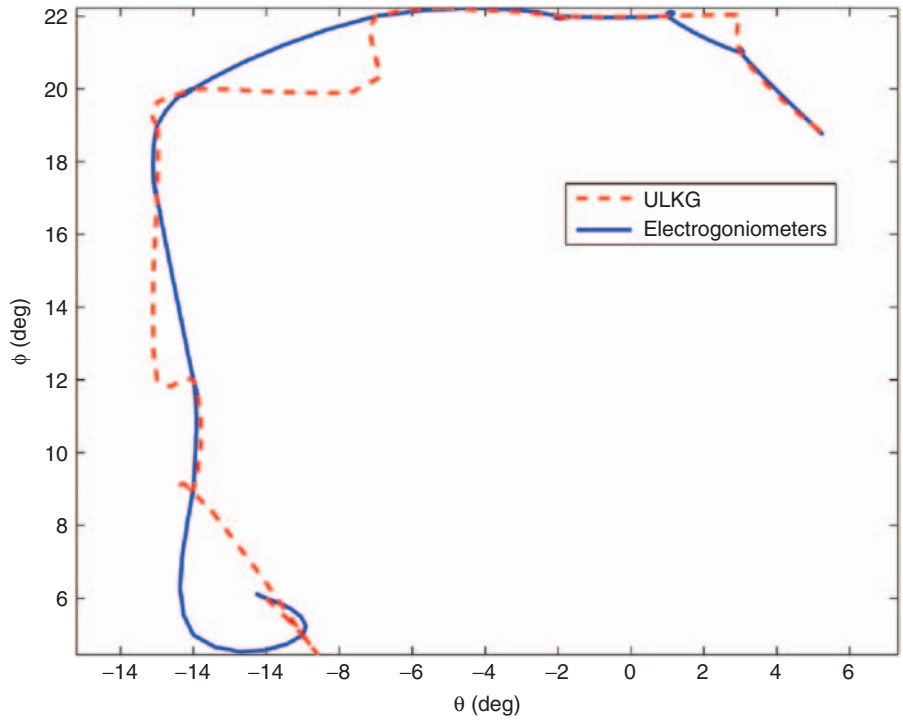

Figure 20 Composition of the flexion angle (abscissa) and abduction angle (ordinates) of the wrist. The continuous line represents the goniometer output, while the dashed one represents the ULKG response

are not capable of detecting them and an identification of the ULKG along this movement direction has not been possible.

6.2.2 Sensing glove: The sensing glove, in its posture detection functionality, has been tested in movements involving the metacarpo-phalangeal joint (in flexion–extension), the proximal interphalangeal joints and the distal interphalangeal joint of the forefinger. Some of these data are collected in Table 3. The average error percentage in detecting the angle is about 4%. In this case, the real angles are measured by using an appropriate electro-goniometer set (Figure 15).

Because of the hand biomechanical complexity, the possibility of sensing glove calibration through electro-goniometers is limited only to a few DOFs. Moreover, electro-goniometers are not firmly fixable over the sensing glove and so they are subject to movement artefacts. For this reasons, more recent trials on the sensing glove have been performed by using a commercial data glove (the Cyberglove® produced by the Immersion Corporation). The Cyberglove® has been used to calibrate our

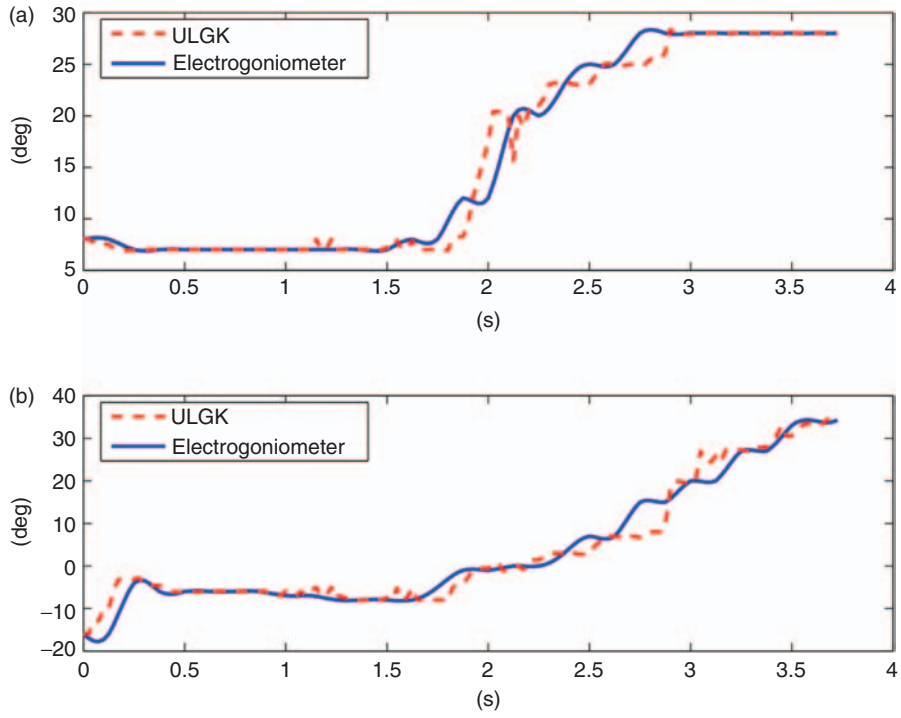

Figure 21 Extension (a) and flexion (b) angles versus time of the shoulder. The continuous line is the goniometer output, while the dashed one represents the ULKG response

prototype in the identification phase and to evaluate performances of the CE sensing glove in detection phase. The results are encouraging and are reported in Figure 24.

7. Discussion

In summary, kinaesthetic garments have shown good results in the output comparison with commercial electro-goniometers. Two kinds of divergence between kinaesthetic garments' behaviour and the goniometer responses are indicated by the introduced diagrams. The first error we can note is a real divergence between the information deriving from the two measurement systems. Trajectories estimate differ for a certain quantity and this phenomenon can be observed both in angle-versus-time diagrams and in terms of trajectories. This is clearly shown in Figure 20 in the range [−12, −8] for flexion angle and [4, 8] for abduction angle. Evaluated in the Cartesian norm, the error estimated is smaller than 5%, if compared with the dimension of the entire workspace. The other artefact we can note is a difference between signals in the angle versus time diagrams, which is not detectable by looking at the other representations.

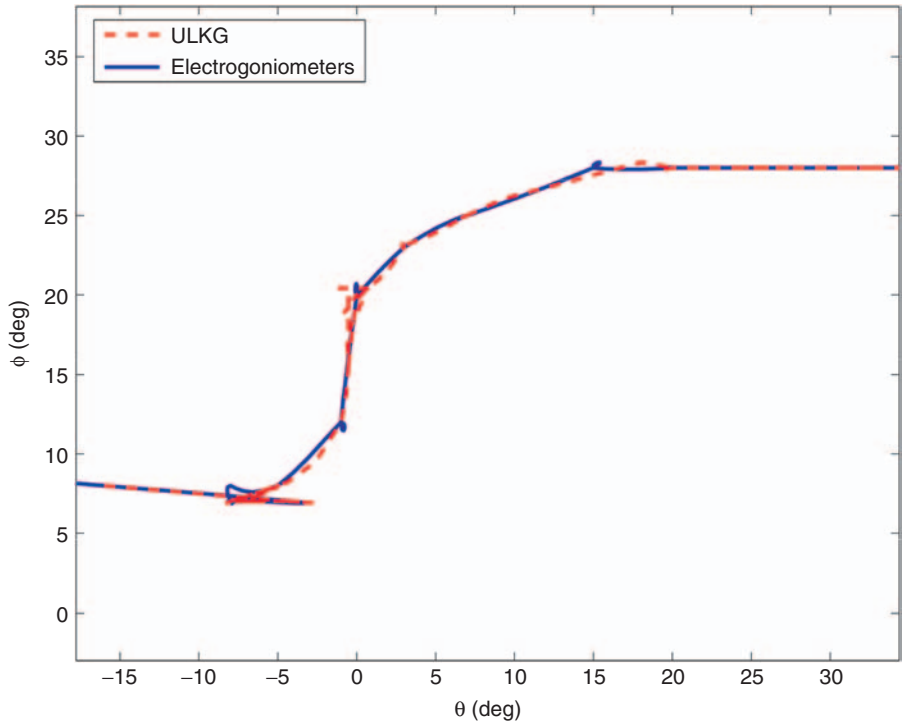

Figure 22 Composition of the flexion angle (abscissa) and extension angle (ordinates) of the shoulder. The continuous line is the goniometer output, while the dashed one represents the ULKG response

This phenomenon is related to a lack of synchronization between the two measurement systems, and it is evident in Figure 21(a) and 21(b) in the [0, 0.5] second range, without corresponding to an effective difference in terms of trajectory, as proved in Figure 22. The two systems produce the same results at different times. A refinement of the movement detection algorithm may avoid these two errors and will be studied in the future. Moreover, a preliminary CE sensing glove validation by using the Cyberglove® has shown encouraging results in the reconstruction of a high number of hand DOFs.

8. Conclusion

In the present work, results from research in the emerging field of textile-based mechano-electrical transducers are presented. Methodologies for the application of fabric CE sensors in the realization of sensorized garments able to detect human gesture, posture and movement have been described. The main advantage introduced

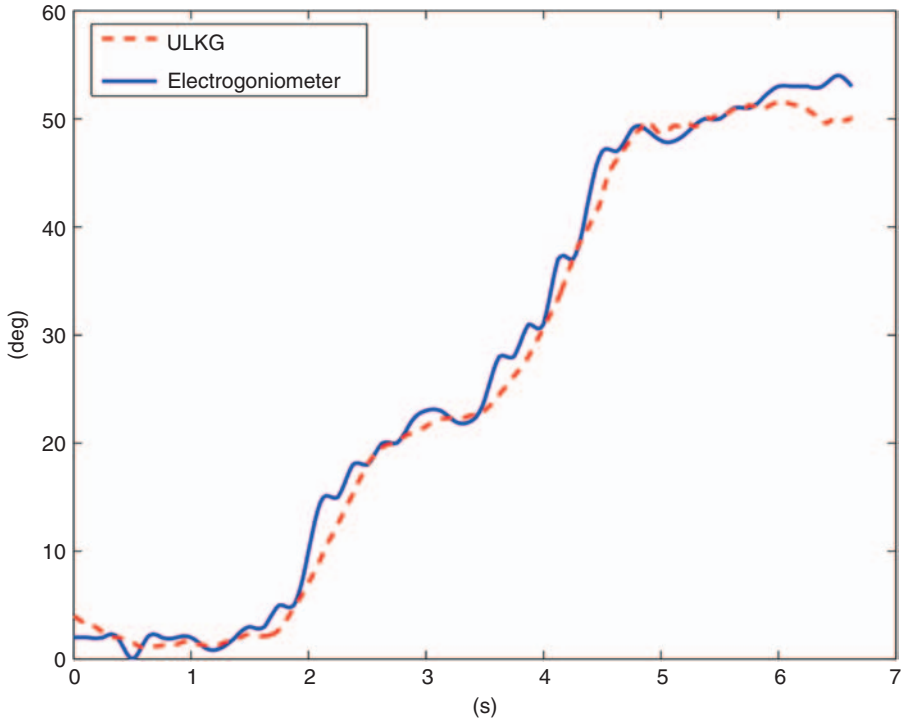

Figure 23 Flexion angle of the elbow. The continuous line is the goniometer output, while the dashed one represents the ULKG response

Table 3 Real and estimated angle values (degrees) for the metacarpophalangeal joint (in flexion–extension), the proximal interphalangeal joints and the distal interphalangeal joint of the forefinger different test points

Real	45	45	0
Estimated	45	45	0
Real	45	22.5	22.5
Estimated	45	25.31	15.47
Real	45	45	45
Estimated	45	42.19	45
Real	75	75	25
Estimated	80.16	67.5	32.34
Real	60	0	0
Estimated	60.47	0	8.44
Real	22.5	22.5	22.5
Estimated	22.5	22.5	22.5

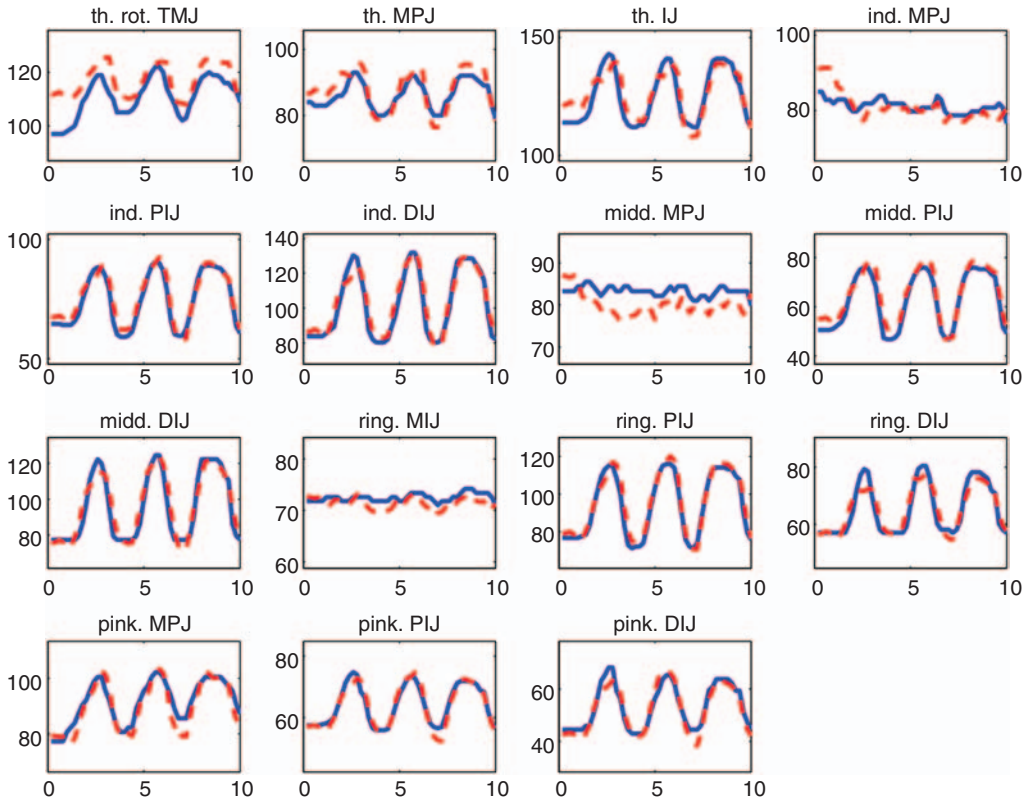

Figure 24 Acquisition of joint angle values for 15 hand DOFs (metacarpo-phalangeal (MPJ), trapezio-metacarpal (TMJ) and interphalangeal (IJ) joints for the thumb, metacarpo-phalangeal (MPJ), proximal interphalangeal (PIJ) and distal interphalalgeal (DIJ) joints for the long fingers). The dashed lines are the CE sensing glove outputs while the continuous lines are Cyberglove® outputs

by the prototypes is their fulfilment of the wearabilty requirements, useful for long-term monitoring. Several issues, deriving from the employment of the illustrated technology, have been addressed. Moreover, it has been pointed out that the use of these sensorized garments is a valid alternative and comfortable instrumentation applicable in several rehabilitation areas, sport disciplines and multimedia fields.

In particular, the production process of the sensing prototypes has been reported and in Section 2, a hardware solution to integrate the CE sensor network in garments without using obtrusive metallic wires as interconnection has been explained. This solution has proved to be a crucial point in effectively employing kinaesthetic garments in real applications.

In Section 3, novel modelling for the behaviour of the sensor employed has been proposed. An algorithm of signal analysis derived from the model has been implemented to consent the use of conductive elastomers as sensors.

Furthermore, the methodology for using the sensorized garments as posture recorders and posture detectors has been introduced in Section 4. We have taken particular care to explain the algorithms necessary to the posture and movement reconstruction. Innovative techniques, whose development has been necessary to ensure good results in garment employment, have been discussed.

Finally, in Section 6, results on the performances of these sensing systems have been reported. Trials conducted on the produced prototypes have shown promising results: the performances of the kinaesthetic garments are comparable with those deriving from conventional measurement systems.

Although kinaesthetic garment performances are very promising, further methodology and technical improvements are necessary. In particular, the refinement of the algorithms for signal analysis and for transient time compensation is a crucial issue. Another important topic is the physical modelling of conductive elastomer fabric sensors. This could provide useful information to improve the performances of the adopted sensors.

Acknowledgements

This research has been funded by the European Commission through PROETEX (IST-4-026987) and MyHeart (IST 507816) projects.

References

Bartalesi, R. 2004: Biomeccanica del movimento: ricostruzione della cinematica corporea tramite sensori cinestetici indossabili. Thesis, University of Pisa.

Biometrics electrogoniometers. www.biometricsltd.com/gonio.htm

Bouten, C.V., **Koekkoek, K.T.**, **Verduin, M.**, **Kodde, R.** and **Janssen, J.D.** 1997: A triaxial accelerometer and portable data processing unit for the assessment of daily physical activity. *IEEE Transactions on Biomedical Engineering* 44, 136–47.

Cyberglove. www.immersion.com/3d/products/cyber_glove.php

De Rossi, D., Carpi, F., Lorussi, F., Mazzoldi, A., Scilingo, E.P. and **Tognetti, A**. 2002: Electroactive fabric for distributed, conformable and interactive systems. *IEEE Sensors 2002 Conference* (*the first IEEE International conference on sensors*), Hyatt Orlando, Kissimmee, FL, June.

De Rossi, D., **Lorussi, F.**, **Mazzoldi, A.**, **Orsini, P.** and **Scilingo, E.P.** 2003: Active dressware: wearable kinesthetic systems. In Barth, F.G., Humphrey, J.A. & Secomb, T.W., editors, *Sensor and sensing in biology and engineering*. Springer-Verlag, 379–92.

Dunne, L.E., **Brady, S.**, **Smyth, B.** and **Diamond, D.** 2005a: Initial development and testing of a novel foam-based pressure sensor for wearable sensing. *Journal of NeuroEngineering and Rehabilitation* 2, March.

Dunne, L.E., Smyth, B., Ashdown, S.P., Sengers, P. and **Kaye, J**. 2005b: Configuring the user in wearable technology design. *Proceedings of the 1st Wearable Futures Conference*, Newport, Wales, September.

Elastosil LR3162 a/b. www.wacker.com

Fontaine, D., David, D. and **Caritu, Y**. 2003: Sourceless human body motion capture. *Smart Objects Conference Symposium*.

Gibbs, P.T. and **Asada, H.H**. 2005: Wearable conductive fiber sensors for multi-axis human joint angle measurement. *Journal of NeuroEngineering and Rehabilitation*, March.

Kapandji, I.A. 2004: *The physiology of the joints – the upper limb*. Churchill Livingstone.

Loriga, G., Taccini, N., De Rossi, D. and **Paradiso, R**. 2005: Textile sensing interfaces for cardiopulmonary signs monitoring. *Proceedings of the* 2005 *IEEE Engineering in Medicine and Biology* 27*th Annual Conference*, Shanghai, September.

Lorussi, F. 2003: Analysis and synthesis of human movement: wearable kinesthetic interfaces. PhD thesis, DSEA, University of Pisa.

Lorussi, F., Rocchia, W., Scilingo, E.P., Tognetti, A. and **De Rossi, D.** 2004: Wearable redundant fabric-based sensors arrays for reconstruction of body segment posture. *IEEE Sensors Journal* 4, 807–18.

Lukowicz, P., Junker, H., Staeger, M., von Bueren, T. and **Troester, G**. 2002: WearNET: a distributed multi-sensor system for context aware wearables. In Borriello, G. and Holmquist, L.E., editors, *UbiComp 2002: Proceedings of the* 4*th International Conference on Ubiquitous Computing*. Springer: Lecture Notes in Computer Science, September, 361–70.

Lymberis, A. and **De Rossi, D.** 2004: *Wearable ehealth systems for personalised health management – state of the art and future challenges*. IOS Press.

Marculescu, D., Marculescu, R., Zamora, N.H., Stanley-Marbell, P., Khosla, P.K., Park, S., Jayaraman, S., Jung, S., Lauterbach, C., Weber, W., Kirstein, T., Cottet, D., Grzyb, J., Tröster, G., Jones, M., Martin, T. and **Nakad, Z**. 2003: Electronic textiles: a platform for pervasive computing. *Proceedings of the IEEE* 91, 1995–2018.

Morris, S.J. and **Paradiso, J.A**. 2002: Shoe-integrated sensor system for wireless gait analysis and real-time feedback. In *Proceedings of the 2nd Joint EMBS/BMES Conference*, October.

Motion tracking tutorial. www.wave-report.com/tutorials/MoTrak.htm

Pappas, I.P.I., Keller, T., Mangold, S., Popovic, M.R., Dietz, V. and **Morari, M.** 2004: A reliable gyroscope-based gait-phase detection sensor embedded in a shoe insole. *IEEE Sensors Journal* 4, 268–74.

Polhemus fastrak. www.polhemus.com/fastrak.htm

Press release. 2004: Adidas introduces the most advanced shoe ever made. www.adidas-salomon.com/en/bizmedia/tool_kits/one/

Scilingo, E.P., Gemignani, A., Paradiso, R., Taccini, N., Ghelarducci, B. and **De Rossi, D.** 2005: Performance evaluation of sensing fabrics for monitoring physiological and biomechanical variables. *IEEE Transactions on Information Technology in Biomedicine* 9, 345–53, September.

Scilingo, E.P., Lorussi, F., Mazzoldi, A. and **De Rossi, D.** 2003: Sensing fabrics for wearable kinaesthetic-like systems. *IEEE Sensors Journal* 3, 460–67.

Shoemake, K. 1987: *Animating rotations with quaternion calculus*. ACM SIGGRAPH.

Steele, J. and **Wallace, G.** 2002: The intelligent knee sleeve: a valid and reliable device to combat ACL injuries. *Journal of Science and Medicine in Sport* 10.

Taya, M., Kim, W.J. and **Ono, K.** 1998: Piezoresistivity of a short fiber/elastomer matrix composite. *Mechanics of Materials* 28, 53–59.

Tognetti, A., Lorussi, F., Bartalesi, R., Quaglini, S., Tesconi, M., Zupone, G. and **De Rossi, D.** 2005: Wearable kinesthetic system for capturing and classifying upper limb gesture in post-stroke rehabilitation. *Journal of NeuroEngineering and Rehabilitation* 2, March.

Tognetti, A., Lorussi, F., Tesconi, M. and **De Rossi, D**. 2004: Strain sensing fabric characterization. In *Third IEEE Sensors Conference*, Vienna.

Tolani, D., Goswami, A. and **Badler, N.I.** 2000: Real-time inverse kinematics techniques for anthropomorphic limbs. *Graphical Models and Image Processing* 62, 353–88.

Van Laerhoven, K., Kern, N., Schiele, B. and **Gellersen, H.W**. 2003: Towards a wearable inertial sensor network. In *Proceedings of the IEE Eurowearable*.

Van Laerhoven, K., Schmidt, A. and **Gellersen, H.W**. 2002: Multi-sensor context-aware clothing. In *Proceedings of the Sixth*

International Symposium on Wearable Computers.

Veldhuizen, TL. 1998: Grid filters for local nonlinear image restoration. M.A.Sc. Thesis, University of Waterloo, Waterloo, Ontario.

Vicon motion systems. www.vicon.com

Wijesiriwardana, R., Dias, T. and **Mukhopadhyay, S**. 2003: Resistive fibre-meshed transducers. *Proceedings of the IEEE 7th International Symposium on Wearable Computers* (*ISWC'03*).

Wijesiriwardana, R., Mitcham, K. and **Dias, T**. 2004: Fibre-meshed transducers based real time wearable physiological information monitoring system. *Proceedings of the Eighth IEEE International Symposium on Wearable Computers* (*ISWC'*04), 40–47.

Zakotnik, J., Matheson, T. and **Volker, D.** 2004: A posture optimization algorithm for model based motion capture of movement sequences. *Journal of Neuroscience Methods* 135, 43–54.